Received: 16 November 2021 | Revised: 14 April 2022 | Accepted: 13 June 2022

DOI: 10.4218/etrij.2021-0285

ORIGINAL ARTICLE

ETRI Journal WILEY

Blind signal separation for coprime planar arrays: An improved coupled trilinear decomposition method

Zhongyuan Que[1,2] | **Xiaofei Zhang**[1] | **Benzhou Jin**[1]

[1]College of Electronic and Information Engineering, Nanjing University of Aeronautics and Astronautics, Nanjing, China

[2]China Mobile Group Guangxi Company Limited, Nanning, China

Correspondence
Xiaofei Zhang, College of Electronic and Information Engineering, Nanjing University of Aeronautics and Astronautics, Nanjing, China.
Email: zhangxiaofei@nuaa.edu.cn

Funding information
National Natural Science Foundation of China, Grant/Award Numbers: 61631020, 61971217, 61971218; National Natural Science Foundation of Jiangsu, Grant/Award Number: BK20200444; Jiangsu Key Research and Development Project, Grant/Award Number: BE2020101

Abstract

In this study, the problem of blind signal separation for coprime planar arrays is investigated. For coprime planar arrays comprising two uniform rectangular subarrays, we link the signal separation to the tensor-based model called coupled canonical polyadic decomposition (CPD) and propose an improved coupled trilinear decomposition approach. The output data of coprime planar arrays are modeled as a coupled tensor set that can be further interpreted as a coupled CPD model, allowing a signal separation to be achieved using coupled trilinear alternating least squares (TALS). Furthermore, in the procedure of the coupled TALS, a Vandermonde structure enforcing approach is explicitly applied, which is shown to ensure fast convergence. The results of Monto Carlo simulations show that our proposed algorithm has the same separation accuracy as the basic coupled TALS but with a faster convergence speed.

KEYWORDS

alternating least squares, coprime planar array, coupled canonical polyadic decomposition, signal separation, tensor decompositions

1 | INTRODUCTION

Blind signal separation is a crucial topic in various engineering fields, such as radar, sonar, wireless communication, and medical diagnosis. It can be interpreted as a procedure of exploiting numerous sensors to simultaneously obtain a mixture of multiple source signals and recover source signals from the mixture without knowing signal propagation conditions [1]. This topic has attracted considerable attention in the past decades, and numerous available algorithms have been proposed. Generally, these algorithms can be coarsely divided into two types; one is the algorithms based on array signal processing techniques, including beamforming [2,3], multiple signal classification (MUSIC) [4,5], and estimating signal parameters via rotational invariance techniques (ESPRIT) [6]; the other is the algorithms based on the independence of the source signals, including fast independent component analysis (Fast-ICA) [7], second-order blind identification (SOBI) [8], and joint approximation diagonalization of eigenmatrices (JADE) [9]. Compared with the latter, the former uses known array geometry and can achieve higher accuracy of signal separation with fewer signal samples, thus attracting more attention in fields such as wireless communication and radar.

Most of the existing studies on signal separation for sensor arrays primarily focus on traditional array geometries, including uniform linear arrays (ULA), uniform circular arrays, and uniform planar arrays [10–12]. The interelement spacing of these arrays needs to be no more than half a wavelength to satisfy Nyquist's sampling theorem, so the array aperture is relatively limited.

Furthermore, there may be severe mutual coupling effects because of the close distance of the elements. Recently, researchers have shifted their research focus from uniform arrays to nonuniform sparse arrays to overcome the limitations of traditional arrays, such as coprime arrays [13,14].

The coprime array is an emerging type of nonuniform sparse array that can achieve large array apertures at low hardware cost, providing significant advantages over conventional arrays. Although studies on coprime arrays are just in their infancy, researchers have already proposed numerous high-precision signal parameters estimation algorithms. In Zhou and others [15], to estimate the direction of arrival (DOA), a spectral search-based approach for coprime linear arrays was proposed by capitalizing on the results of linear subarrays. A search-free 1-D DOA algorithm was proposed in Weng and Djurić [16] for coprime linear arrays using a projection-like approach. In Wu and others [17], a coprime planar array comprising two uniform square subarrays was used, and the conventional 2-D MUSIC algorithm was used for 2-D DOA estimation. In Zheng and others [18], a generalized coprime planar array geometry was developed, and the classical 2-D DOA estimation algorithms such as 2-D MUSIC and 2-D ESPRIT can be performed accompanying ambiguity elimination. However, there are only a few research findings related to signal separation for coprime arrays. In Gu and others [19], a coprime linear array adaptive beamforming algorithm was proposed by establishing a connection between the coprime array and its derived virtual ULA and performance increment can be obtained by processing the equivalent virtual ULA employing existing adaptive beamforming algorithms. In Zhou and others [20], a novel coprime array adaptive beamformer was developed for coprime linear arrays based on the MVDR principle. Most of the studies related to signal separation were conducted for coprime linear arrays, while it is also crucial for practical applications to find effective signal separation approaches for coprime planar arrays.

Recently, the tensor decomposition approach application has developed quickly in sensor array processing, wireless communication, radar signal processing, and independent component analysis [21–26]. As high-order analogs of matrices, tensors possess the inherent multilinear structure and thus have unique advantages in data modeling. Numerous problems in signal processing can be formulated as a canonical polyadic decomposition (CPD) or parallel factor (PARAFAC) decomposition problem by exploiting the signal model structure and properties. The CPD modeling solution can be admitted, but with the limit of ignoring the inherent relation between different arrays for multiple sensor arrays. This limitation can be overcome by a novel tensor-based model called coupled canonical polyadic decomposition [27–29]. Adopting coupled alternating least squares, coupled CPD has the same characteristics of simple computation as the standard CPD but better signal separation performance. Coupled CPD model is a good candidate for achieving signal separation considering the coprime planar arrays feature.

Motivated by the studies mentioned above, in this study, we propose an improved coupled trilinear decomposition approach for the signal separation with a coprime planar array. Specifically, we employ coupled CPD to resolve the signal separation problem for coprime planar arrays and proposed an enhanced signal separation algorithm for coprime planar arrays based on the basic trilinear alternating least squares (TALS). Vandermonde structure characteristic is used in the procedure of coupled trilinear decomposition; thus, compared with the base coupled trilinear decomposition and subarray independent TALS, the proposed algorithm has a better convergence speed. The experimental results show the effectiveness of our algorithm. In this study, we use the generalized coprime planar array in Zheng and others [18].

The primary contributions of this study are summarized as follows:

1. We formulate the signal separation problem for coprime planar arrays as a coupled CPD problem, which can capitalize on the feature of the subarray-shared source matrix to enhance the separation accuracy.
2. We propose an enhanced coupled trilinear decomposition approach, which uses the Vandermonde structure characteristic to speed the coupled trilinear decomposition and resolve scale ambiguity in the decomposition.
3. We examine the proposed approach's computational complexity and verify our approach's superiority by simulation experiments. The findings show that our approach is computationally efficient.

The rest of this study is outlined as follows. The notations used throughout this text are given in the rest of this section. Next, in Section 2, the signal model of a coprime planar array and a coupled CPD model for source separation are introduced. Section 3 reviews the basic coupled TALS approach and presents the proposed algorithm subsequently. The complexity analysis and the advantages of our algorithm are also discussed in Section 3. In Section 4, the results of numerical experiments are presented, and the conclusions are drawn in Section 5.

Notation: Lower-case boldfaces (e.g., $\mathbf{a}$), upper-case boldfaces (e.g., $\mathbf{A}$), and upper-case calligraphic boldfaces

(e.g., $\mathcal{A}$) denote vectors, matrices, and tensors, respectively. $\mathbb{C}$ denotes the sets of complex numbers. The superscripts $(\cdot)^*$, $(\cdot)^{\mathrm{T}}$, $(\cdot)^{\mathrm{H}}$, $(\cdot)^{-1}$, and $(\cdot)^{\dagger}$ represent conjugate, transpose, conjugate transpose, inverse, and Moore–Penrose pseudo-inverse of a vector or matrix, respectively. The symbols $\otimes$ and $\odot$ denote the Kronecker product and Khatri–Rao product. $\|\cdot\|_{\mathrm{F}}$ denotes for the Frobenius norm. The symbol $\circ$ denotes the outer product of vectors, for example, $\mathbf{a}\circ\mathbf{b}\circ\mathbf{c}$. A hat atop stands for estimates, for example, $\hat{\mathbf{a}}$.

2 | DATA MODEL

2.1 | Signal model of coprime planar array

Consider a generalized coprime planar array (GCPA) [18], which is composed of two uniform rectangular subarrays equipped with $N_1 \times M_1$ and $N_2 \times M_2$ sensors, where N_1 and N_2 represent the numbers of sensors on the x-axis while M_1 and M_2 represent the numbers of sensors on the y-axis. N_1 and N_2 are coprime integers as well as M_1 and M_2. The two subarrays have only one common sensor at the origin, and the adjacent distances between sensors in subarray 1 are $d_x^{(1)} = N_2\lambda/2$ and $d_y^{(1)} = M_2\lambda/2$, while the intersensor spacings of subarray 2 are taken as $d_x^{(2)} = N_1\lambda/2$ and $d_y^{(2)} = M_1\lambda/2$, where λ represents the wavelength. Figure 1 shows a simple example of the GCPA.

Assume that R far-field narrowband uncorrelated signals are simultaneously impinging on a GCPA. Let $s_r(t) \in \mathbb{C}$, for $r = 1,...,R$, $t = 0,1,...,$ represents the rth source signal. The output of ith subarray ($i \in \{1,2\}$) can then be expressed as [30]

$$\tilde{\mathbf{x}}^{(i)}(t) = \mathbf{A}^{(i)}\mathbf{s}(t) + \mathbf{n}^{(i)}(t), \quad t = 0,1,2,..., \tag{1}$$

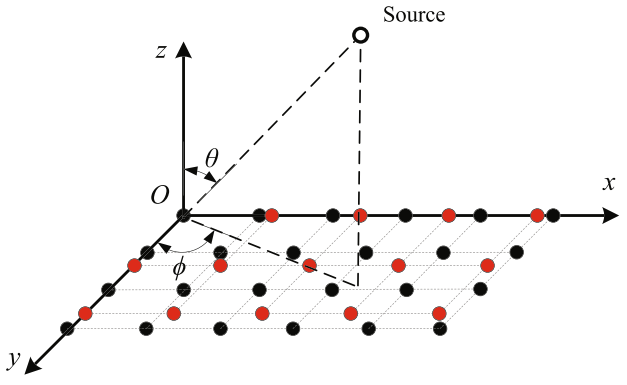

FIGURE 1 The geometry of a generalized coprime planar array, where $N_1 = 5$, $M_1 = 3$, $N_2 = 6$ and $M_2 = 4$

where $\tilde{\mathbf{x}}^{(i)}(t) = [\tilde{x}_1^{(i)}(t), ..., \tilde{x}_{N_iM_i}^{(i)}(t)]^{\mathrm{T}} \in \mathbb{C}^{N_iM_i}$, $\mathbf{s}(t) = [s_1(t), ..., s_R(t)]^{\mathrm{T}} \in \mathbb{C}^R$ represents the vector of source signals, $\mathbf{n}^{(i)}(t) = [n_1^{(i)}(t), ..., n_{N_iM_i}^{(i)}(t)]^{\mathrm{T}} \in \mathbb{C}^{N_iM_i}$ denotes the additive Gaussian i.i.d noise vector, and $\mathbf{A}^{(i)} = [\mathbf{a}_1^{(i)}, ..., \mathbf{a}_R^{(i)}] \in \mathbb{C}^{N_iM_i \times R}$ is the direction matrix consisting of the steering vectors $\mathbf{a}_r^{(i)}$. The steering vector $\mathbf{a}_r^{(i)}$ is related to the geometry of the ith subarray and DOAs of the rth incident signals. For brevity, we assume free space propagation further, and the steering vector $\mathbf{a}_r^{(i)}$ can be given by [30]

$$\mathbf{a}_r^{(i)} = \mathbf{a}_{y,r}^{(i)} \otimes \mathbf{a}_{x,r}^{(i)}, \tag{2}$$

where $\mathbf{a}_{x,r}^{(i)}$, $\mathbf{a}_{y,r}^{(i)}$ represent the steering vectors of the ith subarray along the x-axis and y-axis, which can be written as [17]

$$\mathbf{a}_{x,r}^{(i)} = \left[1, \exp\left(-j2\pi d_x^{(i)} u_r/\lambda\right), ..., \exp\left(-j2\pi(N_i-1)d_x^{(i)} u_r/\lambda\right)\right]^{\mathrm{T}}, \tag{3}$$

$$\mathbf{a}_{y,r}^{(i)} = \left[1, \exp\left(-j2\pi d_y^{(i)} v_r/\lambda\right), ..., \exp\left(-j2\pi(M_i-1)d_y^{(i)} v_r/\lambda\right)\right]^{\mathrm{T}}, \tag{4}$$

where $u_r = \sin\theta_r \cos\phi_r$, $v_r = \sin\theta_r \sin\phi_r$, and θ_r and ϕ_r denote the elevation and azimuth angle, respectively.

Suppose that L snapshots are available, and then the observed data matrix of ith subarray can be compactly expressed as

$$\mathbb{C}^{N_iM_i \times L} \ni \tilde{\mathbf{X}}^{(i)} = \mathbf{A}^{(i)}\mathbf{S} + \mathbf{N}^{(i)} = \left(\mathbf{A}_y^{(i)} \odot \mathbf{A}_x^{(i)}\right)\mathbf{S} + \mathbf{N}^{(i)}, \tag{5}$$

where $\mathbf{A}_y^{(i)} = [\mathbf{a}_{y,1}^{(i)}, ..., \mathbf{a}_{y,R}^{(i)}] \in \mathbb{C}^{M_i \times R}$, $\mathbf{A}_x^{(i)} = [\mathbf{a}_{x,1}^{(i)}, ..., \mathbf{a}_{x,R}^{(i)}] \in \mathbb{C}^{N_i \times R}$, $\mathbf{S} = [\mathbf{s}_1, \mathbf{s}_2, ..., \mathbf{s}_R]^{\mathrm{T}} \in \mathbb{C}^{R \times L}$ denotes source matrix, and $\mathbf{N}^{(i)}$ denotes the corresponding noise matrix.

2.2 | Coupled CPD model for source separation

What we are concerned with in blind source separation is estimating the source matrix $\mathbf{S}$ by observing noisy data $\{\tilde{\mathbf{X}}^{(1)}, \tilde{\mathbf{X}}^{(2)}\}$. The array's geometry can be used to accomplish this purpose. It is easy to notice that (5) is a slice

representation of a three-order tensor that can admit the PARAFAC model or CPD. The CPD writes a tensor $\mathcal{X} \in \mathbb{C}^{I\times J\times K}$ as a sum of rank-1 terms [22]

$$\mathcal{X} = \sum_{r=1}^{R} \mathbf{a}_r \circ \mathbf{b}_r \circ \mathbf{c}_r, \tag{6}$$

where $\mathbf{a}_r \in \mathbb{C}^I$, $\mathbf{b}_r \in \mathbb{C}^J$, and $\mathbf{c}_r \in \mathbb{C}^K$ are the rth columns of factor matrices $\mathbf{A} \in \mathbb{C}^{I\times R}$, $\mathbf{B} \in \mathbb{C}^{J\times R}$, and $\mathbf{C} \in \mathbb{C}^{K\times R}$.

Though CPD can be used to achieve source separation, there is a more appropriate model for GCPA, named coupled CPD. It extends the CPD model to scenarios in which multiple tensors share at least a common factor matrix. A coupled CPD of a set of tensors $\mathcal{X}^{(n)} \in \mathbb{C}^{I_i\times J_i\times K}$, $n \in \{1, \ldots, N\}$, can be expressed as [29]

$$\mathcal{X}^{(n)} = \sum_{r=1}^{R} \mathbf{a}_r^{(n)} \circ \mathbf{b}_r^{(n)} \circ \mathbf{c}_r, \tag{7}$$

where $\mathbf{a}_r^{(n)} \in \mathbb{C}^{I_n}$ and $\mathbf{b}_r^{(n)} \in \mathbb{C}^{J_n}$ are similar to $\mathbf{a}_r$ and $\mathbf{b}_r$ and $\mathbf{c}_r \in \mathbb{C}^K$ is the common vector. Furthermore, the factor matrices are $\mathbf{A}^{(n)} \in \mathbb{C}^{I_n\times R}$, $\mathbf{B}^{(n)} \in \mathbb{C}^{J_n\times R}$, and $\mathbf{C} \in \mathbb{C}^{K\times R}$.

According to the coupled CPD model, we can obtain the tensor form's noiseless observed data for GCPA as

$$\mathbb{C}^{M_i\times N_i\times L} \ni \mathcal{X}^{(i)} = \sum_{r=1}^{R} \mathbf{a}_{y,r}^{(i)} \circ \mathbf{a}_{x,r}^{(i)} \circ \mathbf{s}_r, \quad i \in \{1, 2\}. \tag{8}$$

The coupled CPD of the tensor form is simple, but sometimes it is more convenient to employ its matrix unfolding or slice representation like (5). There are three slice representations of a three-way tensor [29]. Define the horizontal slice matrix $\mathbf{X}^{(m\cdot\cdot,i)} \in \mathbb{C}^{N_i\times L}$ with elements defined as $(\mathbf{X}^{(m\cdot\cdot,i)})_{nl} = (\mathcal{X}^{(i)})_{mnl}$, and we have the following unfolding matrix expressions for GCPA by parallel stacking,

$$\mathbb{C}^{M_iN_i\times L} \ni \mathbf{X}_{(1)}^{(i)} := \begin{bmatrix} \mathbf{X}^{(1\cdot\cdot,i)} \\ \vdots \\ \mathbf{X}^{(M_i\cdot\cdot,i)} \end{bmatrix} = \left(\mathbf{A}_y^{(i)} \odot \mathbf{A}_x^{(i)}\right)\mathbf{S}. \tag{9}$$

Similarly, let $\mathbf{X}^{(\cdot n\cdot,i)} \in \mathbb{C}^{L\times M_i}$ and $\mathbf{X}^{(\cdot\cdot l,i)} \in \mathbb{C}^{M_i\times N_i}$ denote the lateral slice matrix and the frontal slice matrix for which $(\mathbf{X}^{(\cdot n\cdot,i)})_{lm} = (\mathbf{X}^{(\cdot\cdot l,i)})_{mn} = (\mathcal{X}^{(i)})_{mnl}$. Hence, another two unfolding matrices are defined as

$$\mathbb{C}^{N_iL\times M_i} \ni \mathbf{X}_{(2)}^{(i)} := \begin{bmatrix} \mathbf{X}^{(\cdot 1\cdot,i)} \\ \vdots \\ \mathbf{X}^{(\cdot N_i\cdot,i)} \end{bmatrix} = \left(\mathbf{A}_x^{(i)} \odot \mathbf{S}^{\mathrm{T}}\right)\mathbf{A}_y^{(i)\mathrm{T}}, \tag{10}$$

$$\mathbb{C}^{M_iL\times N_i} \ni \mathbf{X}_{(3)}^{(i)} := \begin{bmatrix} \mathbf{X}^{(\cdot\cdot 1,i)} \\ \vdots \\ \mathbf{X}^{(\cdot\cdot L,i)} \end{bmatrix} = \left(\mathbf{S}^{\mathrm{T}} \odot \mathbf{A}_y^{(i)}\right)\mathbf{A}_x^{(i)\mathrm{T}}. \tag{11}$$

In addition to unfolding matrices in (9), (10), and (11), the overall matrix representation of the coupled CPD of $\{\tilde{\mathbf{X}}^{(1)}, \tilde{\mathbf{X}}^{(2)}\}$ is also employed,

$$\mathbb{C}^{(M_1N_1+M_2N_2)\times L} \ni \mathbf{X} := \begin{bmatrix} \mathbf{X}_{(1)}^{(1)} \\ \mathbf{X}_{(1)}^{(2)} \end{bmatrix} = \mathbf{FS}, \tag{12}$$

where $\mathbf{F}$ takes the form as

$$\mathbf{F} = \begin{bmatrix} \mathbf{A}_y^{(1)} \odot \mathbf{A}_x^{(1)} \\ \mathbf{A}_y^{(2)} \odot \mathbf{A}_x^{(2)} \end{bmatrix}. \tag{13}$$

Remark 1. In this study, we assume that the number of sources R is known aforehand, and $R < N_iM_i$.

3 | PROPOSED APPROACH

In this section, we review the standard approach to calculate CPD using coupled TALS algorithm and propose a new coupled TALS algorithm incorporating the Vandermonde structure to accelerate convergence subsequently. The complexity analysis and the proposed approach's advantages are provided at the end of this section.

3.1 | Basic coupled TALS

Numerous algorithms for coupled CPD have been proposed [29], and the coupled TALS approach is the most popular approach among these algorithms. The coupled TALS approach is readily computable and easy to implement. The coupled TALS turns the signal separation problem into the minimization of a quadratic cost function using a least squares criterion:

$$\min_{\mathbf{A}_y^{(1)},\mathbf{A}_y^{(2)},\mathbf{A}_x^{(1)},\mathbf{A}_x^{(2)},\mathbf{S}} \left\| \tilde{\mathcal{X}}^{(1)} - \sum_{r=1}^{R} \mathbf{a}_{y,r}^{(1)} \circ \mathbf{a}_{x,r}^{(1)} \circ \mathbf{s}_r \right\|_{\mathrm{F}}^2 + \left\| \tilde{\mathcal{X}}^{(2)} - \sum_{r=1}^{R} \mathbf{a}_{y,r}^{(2)} \circ \mathbf{a}_{x,r}^{(2)} \circ \mathbf{s}_r \right\|_{\mathrm{F}}^2. \tag{14}$$

In (14), there are five unknown parameters, making the direct computation difficult. The coupled TALS approach uses the multilinearity and coupled property to achieve coupled CPD by alternately updating the estimates of factor matrices. More specifically, the above minimization problem can be equivalently expressed as

$$\min_{\mathbf{A}_y^{(1)},\mathbf{A}_y^{(2)},\mathbf{A}_x^{(1)},\mathbf{A}_x^{(2)},\mathbf{S}} \left\| \tilde{\mathbf{X}} - \mathbf{F}\mathbf{S} \right\|_{\mathrm{F}}^2. \tag{15}$$

Fixing the factor matrices $\mathbf{A}_y^{(1)}$, $\mathbf{A}_y^{(2)}$, $\mathbf{A}_x^{(1)}$, and $\mathbf{A}_x^{(2)}$ to previous estimates $\hat{\mathbf{A}}_y^{(1)}$, $\hat{\mathbf{A}}_y^{(2)}$, $\hat{\mathbf{A}}_x^{(1)}$ and $\hat{\mathbf{A}}_x^{(2)}$, the estimate of coupling factor matrix $\mathbf{S}$ can be attained by

$$\hat{\mathbf{S}} = \hat{\mathbf{F}}^{\dagger}\tilde{\mathbf{X}} = \begin{bmatrix} \hat{\mathbf{A}}_y^{(1)} \odot \hat{\mathbf{A}}_x^{(1)} \\ \hat{\mathbf{A}}_y^{(2)} \odot \hat{\mathbf{A}}_x^{(2)} \end{bmatrix}^{\dagger} \begin{bmatrix} \tilde{\mathbf{X}}_{(1)}^{(1)} \\ \tilde{\mathbf{X}}_{(1)}^{(2)} \end{bmatrix}, \tag{16}$$

where $\tilde{\mathbf{X}}_{(1)}^{(1)}$, $\tilde{\mathbf{X}}_{(1)}^{(2)}$, and $\tilde{\mathbf{X}}$ denote data matrix affected by noise in (9) and (12).

Similarly, the estimation of $\mathbf{A}_y^{(1)}$, $\mathbf{A}_y^{(2)}$, $\mathbf{A}_x^{(1)}$, and $\mathbf{A}_x^{(2)}$ can be achieved by solving the following minimization problem,

$$\min \left\| \tilde{\mathbf{X}}_{(2)}^{(i)} - \left(\mathbf{A}_x^{(i)} \odot \mathbf{S}^{\mathrm{T}} \right) \mathbf{A}_y^{(i)\mathrm{T}} \right\|_{\mathrm{F}}^2, \tag{17}$$

$$\min \left\| \tilde{\mathbf{X}}_{(3)}^{(i)} - \left(\hat{\mathbf{S}}^{\mathrm{T}} \odot \hat{\mathbf{A}}_y^{(i)} \right) \hat{\mathbf{A}}_x^{(i)\mathrm{T}} \right\|_{\mathrm{F}}^2. \tag{18}$$

where $\tilde{\mathbf{X}}_{(2)}^{(i)}$ and $\tilde{\mathbf{X}}_{(3)}^{(i)}$ represent data matrix with noise in (10) and (11), $i \in \{1,2\}$.

Thus, the estimates of $\mathbf{A}_y^{(1)}$, $\mathbf{A}_y^{(2)}$, $\mathbf{A}_x^{(1)}$, and $\mathbf{A}_x^{(2)}$ can be found by the conditional updating

$$\hat{\mathbf{A}}_y^{(i)\mathrm{T}} = \left(\hat{\mathbf{A}}_x^{(i)} \odot \hat{\mathbf{S}}^{\mathrm{T}} \right)^{\dagger} \tilde{\mathbf{X}}_{(2)}^{(i)}, \tag{19}$$

$$\hat{\mathbf{A}}_x^{(i)\mathrm{T}} = \left(\hat{\mathbf{S}}^{\mathrm{T}} \odot \hat{\mathbf{A}}_y^{(i)} \right)^{\dagger} \tilde{\mathbf{X}}_{(3)}^{(i)}, \tag{20}$$

where $\hat{\mathbf{S}}$ represents the current estimate of the factor matrix $\mathbf{S}$ (source matrix).

The coupled TALS approach computes (16), (19), and (20) alternately until convergence. For the first iteration, the factor matrices are randomly initialized.

Remark 2. Similar to most blind separation algorithms, this algorithm also has the problem of permutation and scale ambiguity; thus, the source signals can be estimated in an arbitrary order [28,29].

3.2 | Vandermonde structure enforcing

Though in most situations the basic coupled TALS approach can achieve signal separation, it is observed through simulations that the convergence rate of basic coupled TALS can be enhanced using the signal propagation model's characteristics. Thus, we propose the use of the Vandermonde structure to enhance the algorithm's performance. It is easy to be observed that (3) and (4) are the form of Vandermonde vectors,

$$\mathbf{a}_{y,r}^{(i)} = \left[1, z_{y,r}^{(i)}, \ldots, \left(z_{y,r}^{(i)} \right)^{M_i - 1} \right]^{\mathrm{T}}, \tag{21}$$

$$\mathbf{a}_{x,r}^{(i)} = \left[1, z_{x,r}^{(i)}, \ldots, \left(z_{x,r}^{(i)} \right)^{N_i - 1} \right]^{\mathrm{T}}, \tag{22}$$

where $z_{y,r}^{(i)} = \exp\left(-j2\pi d_y^{(i)} v_r/\lambda\right)$ and $z_{x,r}^{(i)} = \exp\left(-j2\pi d_x^{(i)} u_r/\lambda\right)$, $i \in \{1,2\}$, $r \in \{1, \ldots, R\}$.

Using Vandermonde vector's structural characteristics, we can perform the estimation of $z_{y,r}^{(i)}$ and $z_{x,r}^{(i)}$ in the iteration steps by

$$\hat{z}_{y,r}^{(i)} = \left(\underline{\hat{\mathbf{a}}}_{y,r}^{(i)} \right)^{\dagger} \left(\overline{\hat{\mathbf{a}}}_{y,r}^{(i)} \right), \tag{23}$$

$$\hat{z}_{x,r}^{(i)} = \left(\underline{\hat{\mathbf{a}}}_{x,r}^{(i)} \right)^{\dagger} \left(\overline{\hat{\mathbf{a}}}_{x,r}^{(i)} \right), \tag{24}$$

where $\underline{\hat{\mathbf{a}}}_{y,r}^{(i)}$, $\overline{\hat{\mathbf{a}}}_{y,r}^{(i)}$ are obtained by removing the last and first elements of $\hat{\mathbf{a}}_{y,r}^{(i)}$, the rth column vector of $\hat{\mathbf{A}}_y^{(i)}$; $\underline{\hat{\mathbf{a}}}_{x,r}^{(i)}$, $\overline{\hat{\mathbf{a}}}_{x,r}^{(i)}$ are acquired from $\hat{\mathbf{A}}_x^{(i)}$ in a similar way. After attaining $\hat{z}_{y,r}^{(i)}$ and $\hat{z}_{x,r}^{(i)}$, the new estimates $\hat{\mathbf{a}}_{y,r}^{(i)}$, $\hat{\mathbf{a}}_{x,r}^{(i)}$ can be reconstructed according to (21) and (22). The previous factor matrices $\hat{\mathbf{A}}_y^{(i)}$ and $\hat{\mathbf{A}}_x^{(i)}$ are then substituted by new ones accordingly.

Notably, this Vandermonde structure enforcing scheme overcomes the disadvantage of scaling ambiguities in the basic coupled TALS approach.

The proposed approach's overall procedure is given in Algorithm 1.

Algorithm 1 Coupled Trilinear Alternating Least Squares with Vandermonde Structure Enforcing (CTALS-VDM)

Input: Observed data matrix $\tilde{\mathbf{X}}^{(1)}$, $\tilde{\mathbf{X}}^{(2)}$ from (5).

Initialization:

1. Generate $\hat{\mathbf{A}}_y^{(1)}$, $\hat{\mathbf{A}}_y^{(2)}$, $\hat{\mathbf{A}}_x^{(1)}$, $\hat{\mathbf{A}}_x^{(2)}$ and $\hat{\mathbf{S}}$ randomly.
2. Build unfolding matrix $\tilde{\mathbf{X}}_{(1)}^{(i)}$, $\tilde{\mathbf{X}}_{(2)}^{(i)}$, $\tilde{\mathbf{X}}_{(3)}^{(i)}$, and $\tilde{\mathbf{X}}$ according to (9), (10), (11) and (12), $i \in \{1,2\}$.

Repeat until convergence:

1. Compute $\hat{\mathbf{S}}$ from $\hat{\mathbf{F}}$ and $\tilde{\mathbf{X}}$ according to (16).
2. For each $i \in \{1,2\}$, compute $\hat{\mathbf{A}}_{\mathrm{y}}^{(i)}$ from $\hat{\mathbf{A}}_{\mathrm{x}}^{(i)}$, $\hat{\mathbf{S}}$ and $\tilde{\mathbf{X}}_{(2)}^{(i)}$ according to (19).
3. For each subarray-source pair (i,r), $i \in \{1,2\}$, $r \in \{1,\ldots,R\}$, exploit the Vandermonde structure of the $\hat{\mathbf{A}}_{\mathrm{y}}^{(i)}$ to estimate $\hat{z}_{y,r}^{(i)}$ as in (23), and then rebuild $\hat{\mathbf{a}}_{y,r}^{(i)}$ and $\hat{\mathbf{A}}_y^{(i)}$ according to (21).
4. For each $i \in \{1,2\}$, compute $\hat{\mathbf{A}}_x^{(i)}$ from $\hat{\mathbf{S}}$, $\hat{\mathbf{A}}_y^{(i)}$and $\tilde{\mathbf{X}}_{(3)}^{(i)}$ according to (20).
5. For each subarray-source pair (i,r), $i \in \{1,2\}$, $r \in \{1,\ldots,R\}$, exploit the Vandermonde structure of the $\hat{\mathbf{A}}_{\mathrm{x}}^{(i)}$ to estimate $\hat{z}_{\mathrm{x},r}^{(i)}$ as in (24), and then rebuild $\hat{\mathbf{a}}_{x,r}^{(i)}$ and $\hat{\mathbf{A}}_x^{(i)}$ according to (22).

Output: Estimate of the source matrix $\mathbf{S}$.

Remark 3. There are extra steps, such as computing the cost function to determine whether or not to stop the iteration, in addition to the above computing steps. These steps are not described here because different stop criteria can be used in practice.

Remark 4. The estimates of DOA can also be obtained from $\hat{\mathbf{A}}_x^{(i)}$, $\hat{\mathbf{A}}_y^{(i)}$ via coprime characteristics of the array. Furthermore, the steering vectors for the same source from different subarrays are automatically paired thanks to joint decomposition. The detailed steps to estimate DOA can be found in Zhang and others [26].

3.3 | Complexity analysis

Here, complexity is measured in terms of complex multiplication operations. For brevity, we use the abbreviations ops to refer to complex multiplication operations. From (16), (19), and (20), we conclude that the computational cost of the basic coupled TALS is dominated by computing pseudo-inverses. The first step of computing $\hat{\mathbf{S}}$ requires approximately $R^3+2R^2(M_1N_1+M_2N_2)+(M_1N_1+M_2N_2)RL$ ops. Similarly, the steps of computing $\hat{\mathbf{A}}_y^{(i)}$ and $\hat{\mathbf{A}}_x^{(i)}$, $i\in\{1,2\}$, requires about $2R^3+2R^2(N_1+N_2)L+(M_1N_1+M_2N_2)RL$ ops and $2R^3+2R^2(M_1+M_2)L+(M_1N_1+M_2N_2)RL$ ops, respectively. Then, the total number of ops in each iteration is $5R^3+2R^2(M_1L+M_2L+N_1L+N_2L+M_1N_1+M_2N_2)+3(M_1N_1+M_2N_2)RL$.

Because the proposed approach is based on the basic coupled TALS, the major computational cost is the same. The additional computational cost introduced from (23) and (24) is about $R(3(M_1+M_2+N_1+N_2)-8)$ ops, and the complexity of reconstruction of $\hat{\mathbf{A}}_y^{(i)}$ and $\hat{\mathbf{A}}_x^{(i)}$ is approximately $M_1+M_2+N_1+N_2-8$ ops.

Our approach seems more computational expensive at first glance; however, it is cheaper because the number of total iterations is not considered. The number of iterations to approach convergence varies with different algorithms and depends on numerous factors. As shown in the simulations in the next section, our approach can reduce total iterations and overall time consumption compared with the basic coupled TALS.

3.4 | Advantages

The proposed approach has the following advantages:

1. The proposed approach outperforms the independent TALS approach in terms of signal separation accuracy.
2. The proposed approach has lower computational complexity than the independent TALS and basic coupled TALS approaches.
3. The proposed approach requires no parameter tuning and is still efficient when signals have close DOAs.

4 | NUMERICAL EXPERIMENTS

In this section, we show the proposed approach's signal separation performance for a GCPA by numerical experiments. Consider $R=4$ narrowband far-field signals received by a GCPA, whose output sampling rate is 100 MHz. Table 1 shows the mathematical expressions and DOAs of the source signals.

TABLE 1 Mathematical expressions and incident angles of the source signals

	Mathematical expressions	Elevation	Azimuth
Signal 1	$\cos(2\pi \times 6 \times 10^6 t)$	$\theta_1 = 10^\circ$	$\phi_1 = 15^\circ$
Signal 2	$\cos(\pi \times 8 \times 10^{11} t^2 + 2\pi \times 2 \times 10^6 t)$	$\theta_2 = 20^\circ$	$\phi_2 = 25^\circ$
Signal 3	$\cos(2\pi \times 4 \times 10^5 t)\cos(2\pi \times 5 \times 10^6 t)$	$\theta_3 = 30^\circ$	$\phi_3 = 35^\circ$
Signal 4	$\cos(2\pi \times (4 \times 10^6 + 8 \times 10^4 \cos(\pi \times 3 \times 10^5 t))t)$	$\theta_4 = 40^\circ$	$\phi_4 = 45^\circ$

The experiments are performed using the coprime planar array's signal model described in Section 2 without considering the mutual coupling effect and array error. The number of the elements of subarray 1 is $N_1 = 5$ and $M_1 = 3$, while the number of elements of subarray 2 is $N_2 = 6$ and $M_2 = 4$. Assume that the observed data of the matrix form obtained from the output of subarrays is $\tilde{\mathbf{X}}_{(1)}^{(i)} = \mathbf{X}_{(1)}^{(i)} + \mathbf{N}_{(1)}^{(i)}$, $i \in \{1,2\}$, where $\mathbf{X}_{(1)}^{(i)}$ is the noise-free observed matrix and $\mathbf{N}_{(1)}^{(i)}$ is the additive zero-mean complex Gaussian noise matrix. The signal-to-noise ratio is then defined as follows:

$$\text{SNR}\,[\text{dB}] = 10\log_{10}\left(\sum_{i=1}^{2}\left|\mathbf{X}_{(1)}^{(i)}\right|_F^2 / \sum_{i=1}^{2}\left|\mathbf{N}_{(1)}^{(i)}\right|_F^2\right).$$

We compare the proposed approach's performance with the basic coupled TALS and the subarray independent TALS. For brevity, the approaches will be referred to as CTALS-VDM, CTALS-Basic, and TALS, respectively. The algorithms' separation accuracy is evaluated using the relative error between source matrices and their estimates. The relative error is defined as follows:

$$\text{error} = \min_{\mathbf{\Pi\Lambda}} \left\|\mathbf{S} - \hat{\mathbf{S}}\mathbf{\Pi\Lambda}\right\|_F / \|\mathbf{S}\|_F,$$

where $\mathbf{\Lambda}$ and $\mathbf{\Pi}$ represent the optimally diagonal matrix and permutation matrix, respectively, for solving the scale and permutation ambiguity problems in the decomposition. This relative error was computed using cpderr.m in the tensorlab 3.0 [31]. Furthermore, to compare the algorithms' time complexity, we recorded the running time of different algorithms using the built-in function tic ⧵ toc in MATLAB.

Define cost function as the residual sum of squares, $\psi(k) = \sum_{i=1}^{2}\left\|\tilde{\mathbf{X}}_{(1)}^{(i)} - \hat{\mathbf{X}}_{(1)}^{(i,k)}\right\|_F^2$, where $\hat{\mathbf{X}}_{(1)}^{(i,k)}$ denotes the unfolding matrix of the estimate of tensor $\mathcal{X}^{(i)}$ at the kth iteration. The algorithms are considered convergent when $|\psi(k+1) - \psi(k)|/\psi(k) < \epsilon = 1e-8$. The algorithm is terminated even if the convergence condition is not satisfied when the number of iterations exceeds 2000.

Figure 2A illustrates the time-domain waveforms of source signals, while the time-domain waveforms of separated signals obtained by the proposed algorithm are illustrated in Figure 2B, for snapshots $L = 600$ and SNR = 5 dB. The proposed algorithm can separate source signals accurately without visible distortion.

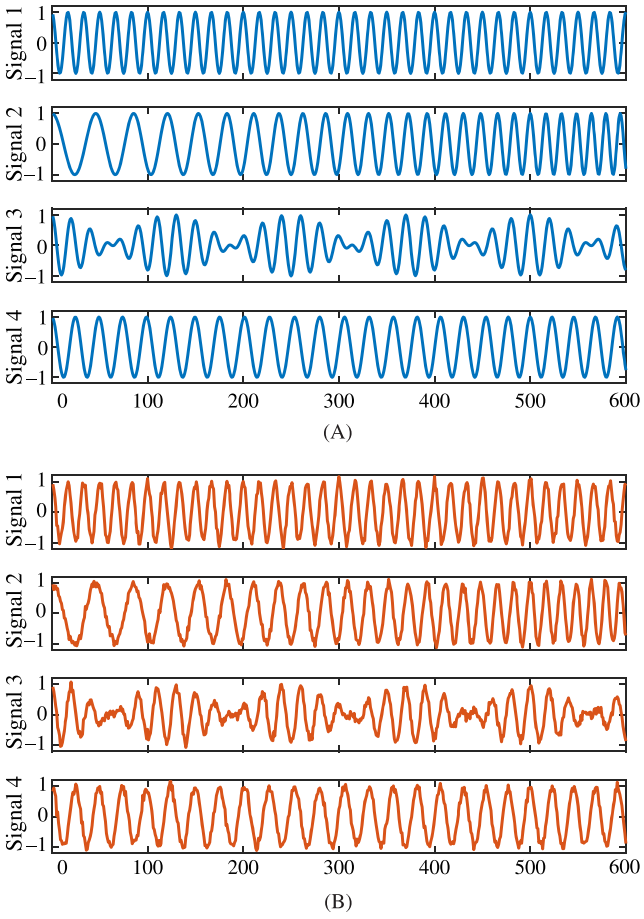

FIGURE 2 Simulated source signals and the separated signals by the proposed method (SNR = 5 dB; $L = 600$): (A) The time-domain waveforms of the source signals and (B) the time-domain waveforms of the separated signals

Figures 3 and 4 show the comparison of the accuracy and the computational cost, respectively, among the algorithms versus SNR for snapshots $L = 1000$, with 400 Monte Carlo trials for each SNR. As shown in Figure 3, the separation error of CTALS-VDM and CTALS-Basic is less than that of TALS-Subarray. This result is as expected because CTALS-VDM and CTALS-Basic make full use of the entire array's information. As

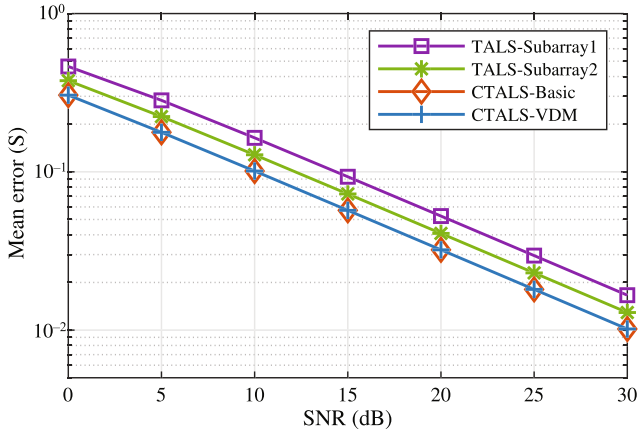

FIGURE 3 Accuracy of different algorithms over 400 trials versus SNR ($L = 1000$)

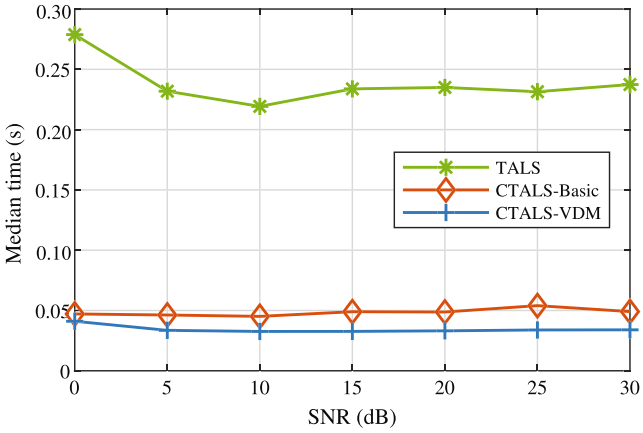

FIGURE 4 Computation time of different algorithms over 400 trials versus SNR ($L = 1000$)

shown in Figure 4, the CTALS-VDM requires the least computation time compared with other algorithms. The time required by TALS here is defined as the sum of the time for two subarrays, and it is significantly longer than the time required for CTALS-VDM and CTALS-Basic, implying that the coupled CPD model can considerably reduce computational cost.

We provide a detailed complexity analysis of the findings for the experiments shown in Figure 4 to further clarify the proposed approach's improvement in computational complexity. The median and mean number of iterations of CTALS-Basic and CTALS-VDM versus SNR are compared in Figure 5A and Figure 5B, respectively. As shown in Figure 5, the median number of iterations of CTALS-Basic and CTALS-VDM are approximately 20 and 13, respectively, while the mean number of iterations of CTALS-Basic and CTALS-VDM are around 64 and 14. The mean number of iterations of CTALS-Basic is substantially higher than the median value,

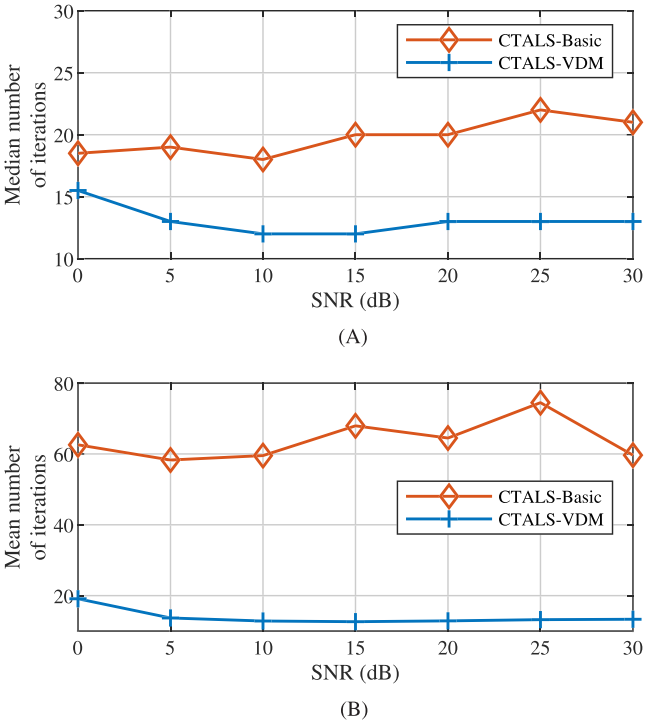

FIGURE 5 The number of iterations of CTALS-Basic and CTALS-VDM over 400 trials versus SNR ($L = 1000$): (A) Median number of iterations and (B) mean number of iterations

implying that the number of iterations required by CTALS-Basic has a larger fluctuation range. However, the median and mean number of iterations of CTALS-VDM are quite close and smaller than those of CTALS-Basic, indicating that it is more stable and excellent in terms of computation time. Typical cost function curves for one trial of Figure 4 when SNR = 5 dB are shown in Figure 6. CTALS-VDM reaches the convergence condition faster than CTALS-Basic.

Figure 7 shows the comparison of the separation accuracy performance among the algorithms with different snapshots L, where SNR = 10 dB and the number of Monte Carlo trials at different snapshots is 200. As shown in Figure 7, the separation accuracy of CTALS-VDM and CTALS-Basic at different snapshots is better than that of subarray independent TALS. The curves of each algorithm in Figure 7 are approximated as lines with zero slopes, implying that the length of the data affects separation accuracy little and that more signal samples do not enhance the accuracy of signal separation. This finding differs from research results on other well-known blind separation algorithms such as SOBI because the approaches here do not explicitly use the characteristics of signal independence and signal statistics.

Figure 8 compares the computational cost of the algorithms with different snapshots. The computation time of CTALS-VDM is still shorter than the other algorithms at

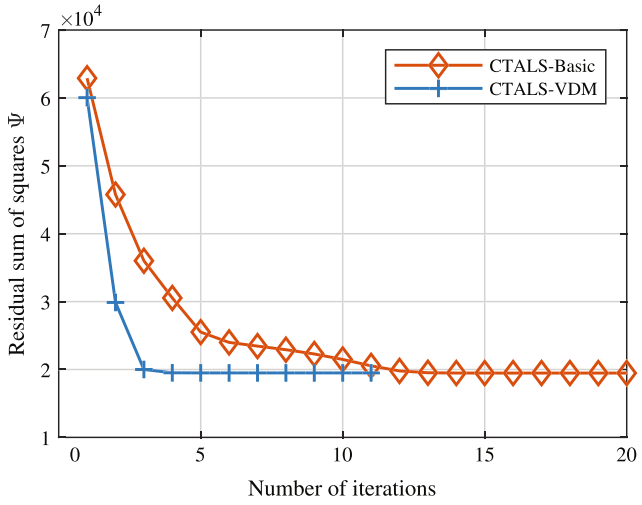

FIGURE 6 The evolution curves of the residual sum of squares for CTALS-Basic and CTALS-VDM in one trial, (SNR = 5 dB; $L = 1000$)

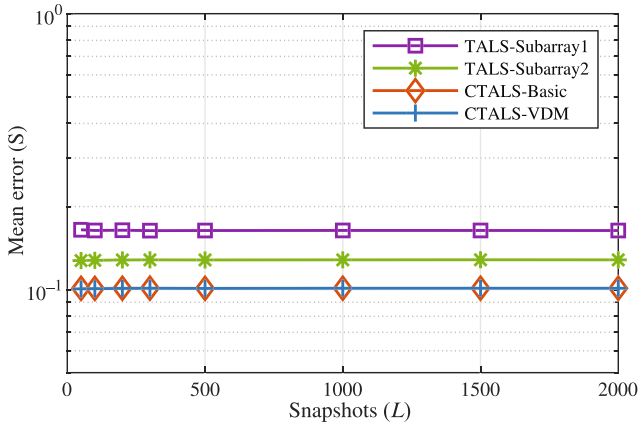

FIGURE 7 Accuracy of different algorithms over 200 trials versus snapshots (SNR = 10 dB)

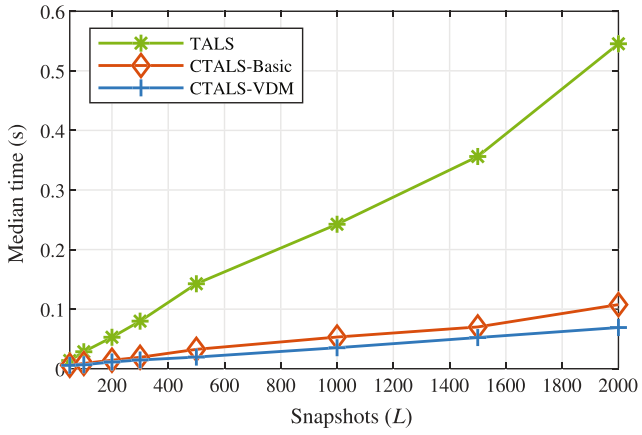

FIGURE 8 Computation time of different algorithms over 200 trials versus snapshots (SNR = 10 dB)

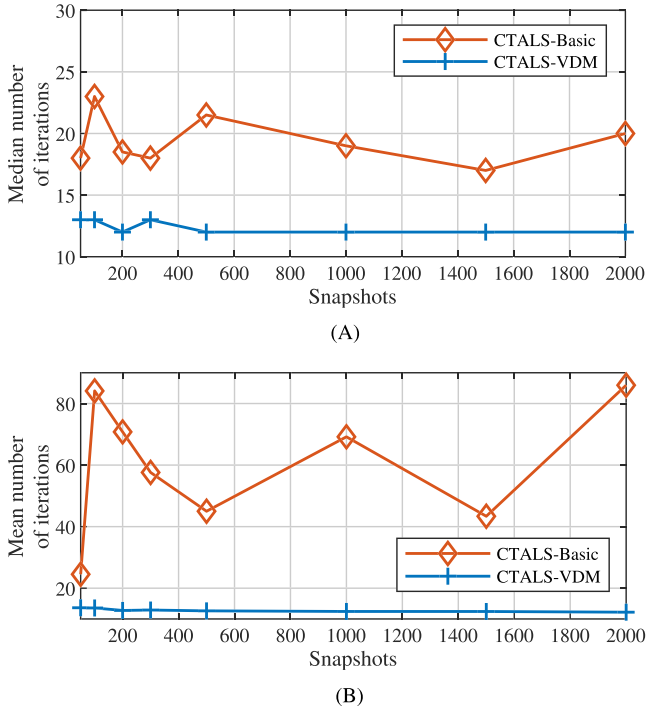

FIGURE 9 The number of iterations of CTALS-Basic and CTALS-VDM over 200 trials versus snapshots (SNR = 10 dB): (A) Median number of iterations and (B) mean number of iterations

different snapshots. The complexity of different algorithms' computation is approximately proportional to snapshots, which is consistent with the findings of our complexity analysis in the previous section. Similarly, we also give a detailed complexity analysis of the the findings for the experiments shown in Figure 8. Figure 9A and Figure 9B compare the median and mean number of iterations, respectively, of CTALS-Basic and CTALS-VDM with different snapshots. The results show that CTALS-VDM is more stable and excellent in terms of computation time for different snapshots and the iterations are slightly affected via snapshots.

To demonstrate the performance of our algorithm when there are closely spaced signals, consider the same source signals as in the previous experiments but with different DOAs. The DOAs of signals 1, 3, and 4 remain the same, while the elevation angle of signal 2, $\theta_2 = \Delta$ varies from 1° to 25° and the azimuth angle $\phi_2 = \Delta + 5°$. The step size of Δ is 0.8°.

In Figure 10, the mean relative error of each algorithm varies with DOA of signal 2 where SNR = 10 dB, the number of snapshots $L = 1000$, and the number of Monte Carlo trials at different angles is 100. As illustrated in Figure 10, when the incidence angle of signal 2 approaches that of signal 1, all algorithms' separation accuracy tends to be worse. However, CTALS-Basic and

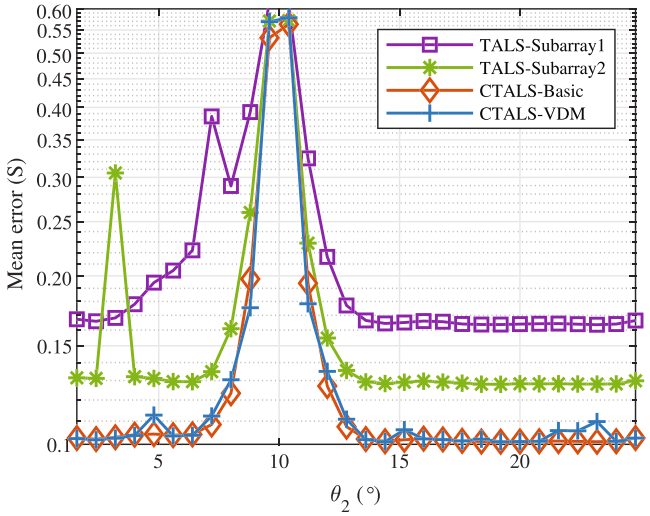

FIGURE 10 Accuracy of different algorithms over 100 trials versus DOA of signal 2 (SNR = 10 dB; $L = 1000$)

CTALS-VDM have narrower peak widths when comparing the angular separation of deterioration for different algorithms, implying that they have better performance in terms of spatial resolution. There are two unusual peaks around $\theta_2 = 3$ and $\theta_2 = 7$ for TALS-Subarray1 and TALS-Subarray2, respectively. The reason for this result is that the approaches of separate subarray processing have the phase ambiguity problem. Though the DOAs of signals are unique, the steering vectors may be close, which may affect the condition of the problem and cause the separation performance to decrease at some particular angles. However, there are no unexpected peaks in the curves of CTALS-Basic and CTALS-VDM, indicating that they have better stability.

5 | CONCLUSIONS

In this study, a blind signal separation issue for coprime planar arrays has been considered. This problem has been formulated as a coupled CPD problem using the fact that subarrays share the same source matrix. This novel formulation allows full use of the information of the entire array so that improved separation accuracy can be attained through coupled CPD. A novel coupled TALS using the Vandermonde structure enforcing approach has been proposed to deal with the time complexity. The simulation experiments reveal that our proposed algorithm is more efficient than basic coupled TALS when using Vandermonde structure characteristics in the procedure of alternating conditional least squares. Furthermore, as demonstrated in simulations, our proposed approach is more stable compared with separate subarray processing.

ACKNOWLEDGMENTS

This work was supported by National Natural Science Foundation of China (Grants 61971217, 61971218, and 61631020), National Natural Science Foundation of Jiangsu (Grant BK20200444), the fund of Sonar Technology Key Laboratory (Research on the theory and algorithm of signal processing for two-dimensional underwater acoustics coprime array) and the fund of Sonar Technology Key Laboratory (Range estimate and location technology of passive target via multiple array combination), and Jiangsu Key Research and Development Project (Grant BE2020101).

CONFLICT OF INTEREST

The author declares that there are no conflicts of interest.

ORCID

Zhongyuan Que https://orcid.org/0000-0002-2653-4305

REFERENCES

1. C. Jutten and P. Comon, *Chapter 1—Introduction*, *Handbook of Blind Source Separation*, P. Comon and C. Jutten, (eds.), Academic Press, Oxford, 2010, pp. 1–22.
2. J. Li, P. Stoica, and Z. Wang, *On robust Capon beamforming and diagonal loading*, (IEEE International Conference on Acoustics, Speech, and Signal Processing, 2003. Proceedings, Hong Kong, China), Apr. 2003. https://doi.org/10.1109/ICASSP.2003.1199947
3. X. Zhang and D. Xu, *Angle estimation in bistatic MIMO radar using improved reduced dimension Capon algorithm*, J. Syst. Eng. Electron. **24** (2013), no. 1, 84–89.
4. R. Schmidt, *Multiple emitter location and signal parameter estimation*, IEEE Trans. Antennas Propag. **34** (1986), no. 3, 276–280.
5. X. Zhang, L. Xu, L. Xu, and D. Xu, *Direction of Departure (DOD) and Direction of Arrival (DOA) estimation in MIMO radar with reduced-dimension MUSIC*, IEEE Commun. Lett. **14** (2010), no. 12, 1161–1163.
6. R. Roy and T. Kailath, *ESPRIT-estimation of signal parameters via rotational invariance techniques*, IEEE Trans. Acoust. Speech Signal Process. **37** (1989), no. 7, 984–995.
7. A. Hyvärinen and E. Oja, *A fast fixed-point algorithm for independent component analysis*, Neural Comput. **9** (1997), no. 7, 1483–1492.
8. A. Belouchrani, K. Abed-Meraim, J.-F. Cardoso, and E. Moulines, *A blind source separation technique using second-order statistics*, IEEE Trans. Signal Proc. **45** (1997), no. 2, 434–444.
9. J. F. Cardoso and A. Souloumiac, *Blind beamforming for non-Gaussian signals*, IEE Proc. F. (Radar Signal Process.) **140** (1993), no. 6, 362–370.
10. P. Ioannides and C. A. Balanis, *Uniform circular and rectangular arrays for adaptive beamforming applications*, IEEE Antennas Wirel. Propag. Lett. **4** (2005), 351–354.
11. B. Liao and S.-C. Chan, *Adaptive beamforming for uniform linear arrays with unknown mutual coupling*, IEEE Antennas Wirel. Propag. Lett. **11** (2012), 464–467.

12. Y. Zhou, Z. Fei, S. Yang, J. Kuang, S. Chen, and L. Hanzo, *Joint angle estimation and signal reconstruction for coherently distributed sources in massive MIMO systems based on 2-D unitary ESPRIT*, IEEE Access **5** (2017), 9632–9646.
13. P. P. Vaidyanathan and P. Pal, *Theory of sparse coprime sensing in multiple dimensions*, IEEE Trans. Signal Process. **59** (2011), no. 8, 3592–3608.
14. P. P. Vaidyanathan and P. Pal, *Sparse sensing with co-prime samplers and arrays*, IEEE Trans. Signal Process. **59** (2011), no. 2, 573–586.
15. C. Zhou, Z. Shi, Y. Gu, and X. Shen, *DECOM: DOA estimation with combined MUSIC for coprime array*, (International Conference on Wireless Communications and Signal Processing, Hangzhou, China), Oct. 2013. https://doi.org/10.1109/WCSP.2013.6677080
16. Z. Weng and P. M. Djurić, *A search-free DOA estimation algorithm for coprime arrays*, Digital Signal Process. **24** (2014), 27–33.
17. Q. Wu, F. Sun, P. Lan, G. Ding, and X. Zhang, *Two-dimensional direction-of-arrival estimation for co-prime planar arrays: A partial spectral search approach*, IEEE Sensors J. **16** (2016), no. 14, 5660–5670.
18. W. Zheng, X. Zhang, and H. Zhai, *Generalized coprime planar array geometry for 2-D DOA estimation*, IEEE Commun. Lett. **21** (2017), no. 5, 1075–1078.
19. Y. Gu, C. Zhou, N. A. Goodman, W.-Z. Song, and Z. Shi, *Coprime array adaptive beamforming based on compressive sensing virtual array signal*, (IEEE International Conference on Acoustics, Speech and Signal Processing, Shanghai, China), Mar. 2016. https://doi.org/10.1109/ICASSP.2016.7472224
20. C. Zhou, Y. Gu, S. He, and Z. Shi, *A robust and efficient algorithm for coprime array adaptive beamforming*, IEEE Trans. Veh. Technol. **67** (2018), no. 2, 1099–1112.
21. J. Li and M. Zhou, *Improved trilinear decomposition-based method for angle estimation in multiple-input multiple-output radar*, IET Radar Sonar Navigation **7** (2013), no. 9, 1019–1026. _eprint: https://ietresearch.onlinelibrary.wiley.com/doi/pdf/10.1049/iet-rsn.2012.0345
22. N. D. Sidiropoulos, R. Bro, and G. B. Giannakis, *Parallel factor analysis in sensor array processing*, IEEE Trans. Signal Process. **48** (2000), no. 8, 2377–2388.
23. N. D. Sidiropoulos, G. B. Giannakis, and R. Bro, *Blind PARAFAC receivers for DS-CDMA systems*, IEEE Trans. Signal Process. **48** (2000), no. 3, 810–823.
24. L. Xu, F. Wen, and X. Zhang, *A novel unitary PARAFAC algorithm for joint DOA and frequency estimation*, IEEE Commun. Lett. **23** (2019), no. 4, 660–663.
25. X. Zhang, Z. Xu, L. Xu, and D. Xu, *Trilinear decomposition-based transmit angle and receive angle estimation for multiple-input multiple-output radar*, IET Radar, Sonar Navig. **5** (2011), no. 6, 626–631.
26. X. Zhang, W. Zheng, W. Chen, and Z. Shi, *Two-dimensional DOA estimation for generalized coprime planar arrays: a fast-convergence trilinear decomposition approach*, Multidim. Syst. Sign. Process. **30** (2019), no. 1, 239–256.
27. M. Sorensen, I. Domanov, and L. De Lathauwer, *Coupled canonical polyadic decompositions and multiple shift invariance in array processing*, IEEE Trans. Signal Process. **66** (2018), no. 14, 3665–3680. https://ieeexplore.ieee.org/document/8357500/
28. M. Sørensen and L. D. De Lathauwer, *Coupled canonical polyadic decompositions and (coupled) decompositions in multilinear rank-$(L_r,n,L_r,n,1)$ terms–Part I: Uniqueness*, SIAM J. Matrix Anal. Appl. **36** (2015), no. 2, 496–522. https://doi.org/10.1137/140956853
29. M. Sørensen, I. Domanov, and L. De Lathauwer, *Coupled canonical polyadic decompositions and (coupled) decompositions in multilinear rank- $(L_{r,n},L_{r,n},1)$ terms—Part II: Algorithms*, SIAM J. Matrix Anal. Appl. **36** (2015), no. 3, 1015–1045.
30. Yih-Min Chen, Ju-Hong Lee, and Chien-Chung Yeh, *Two-dimensional angle-of-arrival estimation for uniform planar arrays with sensor position errors*, IEE Proc. F Radar Signal Process. UK **140** (1993), no. 1, 37.
31. N. Vervliet, O. Debals, and L. De Lathauwer, *Tensorlab 3.0 – Numerical optimization strategies for large-scale constrained and coupled matrix/tensor factorization*, (50th Asilomar Conference on Signals, Systems and Computers, Pacific Grove, CA, USA), Nov. 2016. https://doi.org/10.1109/ACSSC.2016.7869679

AUTHOR BIOGRAPHIES

Zhongyuan Que received his BE degree in Electronic Information Engineering from Northeastern University, Shenyang, China, in 2019 and his ME degree in Communication and Information Systems from Nanjing University of Aeronautics and Astronautics, Nanjing, China, in 2022. His research interests include array signal processing.

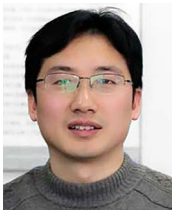

Xiaofei Zhang received his MS degree from Wuhan University, Wuhan, China, in 2001 and his PhD degree in Communication and Information Systems from the Nanjing University of Aeronautics and Astronautics, Nanjing, China, in 2005. He is currently a full professor with the Electronic Engineering Department, Nanjing University of Aeronautics and Astronautics. His research interests include array signal processing and communication signal processing. He is on the technical program committees of the IEEE 2010 International Conference on Wireless Communications and Signal Processing, the IEEE 2011 International Conference on Wireless Communications and Signal Processing, SSME 2010, and 2011 International Workshop on Computation Theory and Information Technology. He is the editor of the *International Journal of Digital Content Technology and its Applications*, the *International Journal of Technology and Applied Science*, the *Journal of Communications and Information Sciences*, the

Scientific Journal of Microelectronics, and the *International Journal of Information Engineering*.

Benzhou Jin received his BE degree in Instrument Science and Technology from Xidian University, Xi'an, China, in 2008 and his PhD degree in Information and Communication Engineering from Tsinghua University, Beijing, China, in 2013. From 2013 to 2018, he was a senior engineer with the Nanjing Research Institute of Electronics Technology, Nanjing, China. Since 2018, he has been an associate professor with the College of Electronic and Information Engineering, Nanjing University of Aeronautics and Astronautics, Nanjing, China. His current research interests include radar system engineering, nonlinear signal processing, and array signal processing.

How to cite this article: Z. Que, X. Zhang, and B. Jin, *Blind signal separation for coprime planar arrays: An improved coupled trilinear decomposition method*, ETRI Journal **45** (2023), 138–149. https://doi.org/10.4218/etrij.2021-0285